Journal of Energy Storage 72 (2023) 108491

Contents lists available at ScienceDirect

Journal of Energy Storage

journal homepage: www.elsevier.com/locate/est

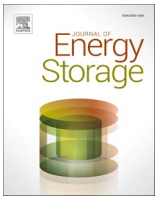

Research papers

AlTiMgLiO medium entropy oxide additive for PEO-based solid polymer electrolytes in lithium ion batteries

Timothy G. Ritter [a], Josué M. Gonçalves [c,d], Stoyan Stoyanov [c], Alireza Ghorbani [c], Tolou Shokuhfar [b], Reza Shahbazian-Yassar [c,*]

[a] Department of Civil & Materials Engineering, University of Illinois Chicago, Chicago, IL 60607, USA
[b] Department of Biomedical Engineering, University of Illinois Chicago, Chicago, IL 60607, USA
[c] Department of Mechanical & Industrial Engineering, University of Illinois Chicago, Chicago, IL 60607, USA
[d] Instituto de Quimica, Universidade de São Paulo, Av. Prof. Lineu Prestes 748, 05508-000 São Paulo, SP, Brazil

ARTICLE INFO

Keywords:
Solid polymer electrolytes
Ionic conductivity
Lithium-ion batteries
Polyethylene oxide
Multielement Oxide
Polymer composites

ABSTRACT

Solid polymer electrolytes (SPE) have attracted considerable attention as electrolytes for solid-state batteries due to their toughness, high safety, and ionic conductivities that can be comparable with liquid electrolytes, especially at higher temperatures. However, polymers have low elastic moduli, which decrease at higher temperatures, limiting their ability to reduce dendrite formation. Mechanical blocking is one method of improving the interfacial layer and reducing dendritic growth but requires the elastic modulus of the polymer to be high enough to suppress lithium dendrites growth. Previous studies have focused on using unary metal oxides, which are limited by the percent of additives that can be included in the polymer before causing negative effects on electrochemical properties. In this study, we demonstrate a new strategy for improving the performance of polymers by synthesizing a multielement oxide (MEO) filler, AlTiMgLiO, to create a composite SPE with enhanced electrochemical performance. The synthesized AlTiMgLiO-containing SPE resulted in a voltage window of 0–6.18 V and a lithium transference number of 0.42. The overpotential voltage during galvanostatic cycling was reduced due to the improvements made to the morphology. The improvement of the interfacial layer reduced Li dendritic growth, resulting in a capacity of 99.68 mAh g^{-1} after 500 cycles, and a capacity retention of 78.69 %. The possible reasons for the improvement are discussed, providing a direction for future studies on the use of multielement materials as fillers in solid polymers electrolytes.

1. Introduction

The use of lithium-ion batteries (LIBs) to power modern conveniences has been increasing over the past two decades. Despite cost reductions, many LIBs are facing more stringent performance requirements such as higher energy density, fast charging capabilities, improved safety, and longer cycling life. Current graphite anodes are nearing their limits to meet these performance demands, and new anodes are required. The ideal anode for future LIB is Li metal due to its high theoretical specific capacity (3860 mAh g^{-1}), light weight (0.59 g cm^{-3}), and lowest negative potential (−3.040 V vs. standard hydrogen electrode) [1]. Unfortunately, due to Li dendrite growth during charge/discharge cycling, the Li metal anode has seen limited commercialized success. The dendritic growth problem can be solved by replacing the liquid electrolytes found in current LIB with solid polymer electrolytes (SPE). SPE are light weight, easy to manufacturer for large-scale production, low cost, and has high mechanical toughness [2–5]. The most promising and widely studied polymer for polymer electrolytes is polyethylene oxide (PEO). One advantage that PEO has over other polymers is its low glass transition (T_g) temperature of −60 °C [6]. In fact, ionic conductivity in PEO is low (10^{-6}–10^{-8} S cm^{-1}) at room temperature due to decreased carrier mobility in the crystalline region and increases above the melting temperature (~60 °C) [7,8]. The amorphous phase of the polymer is the main reason for the migration of ions [7]. Due to the high reactivity of Li metal, reactions can occur at the Li metal|polymer interface resulting in poor electrochemical performance and decreased lifespans [9,10]. During cycling, this interfacial layer growth can lead to uneven morphology, larger impedances, increases in overpotential voltages, poor battery lifespans and Li dendritic growth that can easily pierce the soft SPE [11–13]. While PEO can have

* Corresponding author.
E-mail address: rsyassar@uic.edu (R. Shahbazian-Yassar).

https://doi.org/10.1016/j.est.2023.108491
Received 7 May 2023; Received in revised form 15 July 2023; Accepted 23 July 2023
Available online 12 August 2023

moderate ionic conductivities, it also has a low Young's modulus of 205–633 MPa depending on the molecular weight of the polymer [14]. The highest conductivities are found at higher temperatures (~60 °C) in the amorphous region, while the best mechanical properties are found at lower temperatures (~20 °C) in the crystalline region. Mechanical studies of PEO have shown that the shear modulus of the electrolyte should be twice as high as the Li anode (~10^9 Pa) in order to suppress dendritic growth [1].

To overcome the limitations of PEO, fillers such as TiO_2, Al_2O_3, $LiAlO_2$, and Li_3N have been added to the polymer matrix to increase their electrochemical and mechanical properties [15,16]. The inorganic particles can change the crystallization, mechanical strength, thermal stability, ionic conductivity, and ion transport of the polymers [17–22]. Additionally, compositions such as Lithium Lanthanum Titanate (LLZO) have been employed as additive due to their high ionic conductivities (~10^{-4} S cm^{-1}) [8]. While incorporating additives into the polymer structure can improve mechanical performance by increasing the shear and elastic modulus, at high weight percentages, these additives can cause adverse effects on the electrochemical properties and processability of the polymer [8,15,23].

In this study, we report on the use of a multielement oxide (MEO) as an filler for PEO-based solid polymer electrolytes (SPE). Multielement materials, due to synergestic contributions of elements, have shown to provide high chemical, structural, and electrochemical stability [24,25]. These benefits make multielement materials promising candidates for improving the performance of SPE. In our work, LIBs made from the MEO incorporated SPEs showed capacity of 99.68 mAh g^{-1} after 500 cycles, resulting in a capacity retention of 78.69 % at 1C. The improved properties resulted in a more uniform and stable morphology, resulting is less degradation and higher capacity retention while also increasing and stabilizing the Coulombic efficiency.

2. Materials and methods

2.1. Materials

Polyethylene oxide (PEO) (M_w = 1,000,000), Bis(trifluoromethane) sulfonamide lithium salt (LiTFSI, 99.95 % trace metals basis), and Acetonitrile (≥99.9 %) were purchased from Sigma Aldrich and used as received. The multielement oxide fillers were synthesized using a ball milling and sintering technique [26,27]. Precursors for the MEO (AlTiMgLiO) of aluminum oxide (≥98 % Al_2O_3), titanium (IV) oxide (nanopowder <25 nm, 99.7 %), magnesium oxide (≥99 %, −325 mesh) and lithium carbonate (99.997 %) were purchased from Sigma Aldrich and used as received.

2.2. Preparation of MEO additives

The MEO filler was synthesized using a ball milling and sintering technique. The binary metal oxide precursors were combined in equimolar amounts (0.002 mols) and ball milled using a SPEX SamplePrep Mixer/Mill 8000 M for 300 min. After ball milling, the powder was pressed into a 15 mm pellet at 250 MPa. The pellet was then free sintered in a Thermo Scientific Lindberg Blue M oven at 1020 °C for 12 h. After sintering, the pellet was ball milled back into a powder.

2.3. Preparation of PEO-based solid polymer electrolytes

The PEO-based solid polymers were prepared by a solution casting method. A stock solution of 500 mg of PEO and 181.04 mg of LiTFSI salt was dissolved in acetonitrile. The salt concentration was kept constant in all SPE at EO:Li = 18. Various amounts of the MEO powder were added to each stock solution. Three sets of samples were made for study consisting of no additive, 10 wt% MEO additive, and 60 wt% MEO additive referred to as SPE-0, SPE-MEO-10, and SPE-MEO-60. The polymer with no additive served as a control case. The 10 wt% MEO filler was the result of a concentration study to find the polymer with the highest ionic conductivity at room temperature. The 60 wt% MEO additive SPE was used as an extreme case of additive to study the effects of high concentrations. For additional electrochemical comparison, SPEs were cycled with a unary composition made with 10 wt% fillers of Al_2O_3, referred to as SPE-Al_2O_3–10. The solution was stirred for 8 h at room temperature until well mixed. The slurry was then cast into a Teflon petri dish and dried at 40 °C for 3 h to remove the acetonitrile, then moved to a vacuum oven to dry at 60 °C for 12 h.

2.4. Characterization

Field emission scanning electron microscope (FESEM) and energy dispersive spectroscopy (EDS) measurements were performed on a 30-kV JEOL JSM-IT500HR operated at accelerating voltage of 5 kV. Selected area diffraction pattern (SAED) collection and Energy dispersive spectroscopy (EDS) were performed using an aberration corrected JEOL ARM200CF with a cold field emission gun operated at 200 kV, equipped with an Oxford X-max 100TLE windowless X-ray detector. XRD was performed on a Bruker D8 with a 2θ range of 10° to 85° at 1600 W (40 kV, 40 mA). The resolution was 0.02° with time steps of 1.5 s. The thickness of the SPE was measured at several locations with a Rexbeti digital micrometer with a 0.001 mm resolution.

2.5. Cell assembly

The electrochemical properties of the SPEs were determined after assembly in a CR2032 coin cell in an argon filled glovebox. EIS tests were conducted on SS || SPE || SS cells (where SS refers to stainless steel) as seen in Fig. S1A. The cycling tests were performed on LFP || SPE || Li cells as seen in Fig. S1B with a cathode material composed of $LiFePO_4$ (LFP), Super P carbon black 99 + % and polyvinylidene fluoride (PVDF) by weighed ratios of 70:15:15 and cast onto aluminum foil. *N*-methyl pyrrolidone (NMP) was used as the solvent. The active material loading of LFP was 1.57 mg cm^{-2}. Lithium metal (thickness 0.25 mm) was used as the anode. The SPE was punched into 17 mm discs from the main casting and ranged in thickness from 153 to 247 μm depending on MEO filler amount. The SPE was used directly as the electrolyte and membrane in each cell. The voltage range during cycling was 2.5–4.2 V at a rate of 1C (1C = 160 mAh) and a temperature of 80 °C. The LSV was performed on a Li || SPE || SS cell as seen in Fig. S1C. The over potential test was performed on a Li || SPE || Li cell as seen in Fig. S1D.

2.6. Electrochemical measurements

All testing was performed on a BioLogic VMP3. Cyclic Voltammogram (CV) tests were conducted in a potential window of 2.5–4.2 V at 0.1 mVs^{-1} and a temperature of 80 °C. The ionic conductivity of the SPE was measured using electrochemical impedance spectroscopy (EIS) with a frequency range of 10^6 Hz to 10^{-1} Hz with a 10 mV potential amplitude. The cells were assembled using a 2032 coin cell, two stainless steel blocking electrodes and the SPE in an argon filled glovebox.

The charge/discharge tests were performed in the voltage range of 2.5–4.2 V at 1C (1C = 160 mAh) and a temperature of 80 °C. The lithium ion transference number (t_{Li}^{+}) of the SPE was measured at 80 °C using AC impedance and DC polarization in Li || SPE || Li symmetrical cells. The DC voltage (ΔV) was 10 mV and the impedance was measured between 1 MHz and 0.01 Hz with an oscillation voltage of 10 mV. The over potential of the SPE was measured at 80 °C with a current of 20 μA cm^{-2} and a 60 min charge/discharge cycle [28].

3. Results and discussion

A common method for making polymer electrolytes is to use the casting process. Polymer and MEO fillers were mixed together and then

cast into a sample holder and dried. The casting process is described below in the Experimental Procedures section. The MEO fillers were synthesized using a ball milling and sintering technique, which was chosen based on the desired elements used for the MEO filler. The full process description can be found below in the Experimental Procedures section.

3.1. Structure of AlTiMgLiO MEO powder

The morphology of the MEO fillers and the various SPE were analyzed using SEM and TEM, as shown in Fig. 1A. The particles exhibited an irregularly shaped structure with an average particle size of 204 nm (Fig. S2). A TEM image of the AlTiMgLiO particles is shown in Fig. S3. X-ray diffraction (XRD) was utilized to characterize both the SPE and the MEO additive. The XRD pattern for the AlTiMgLiO MEO powder can be seen in Fig. 1B, which revealed that the synthesized particles can be characterized as a cubic spinel crystal phase with a lattice constant of 8.11 ± 0.02 Å [29,30]. The corresponding selected area electron diffraction (SAED) pattern for the additive powder is depicted in Fig. 1C, which displayed the planes for 111, 220, 311, 400, 420, and 262 that were also found in the XRD results, confirming the spinel crystal structure of the MEO additive. However, additional peaks not attributed to the spinel crystal structure were present in the SAED and XRD pattern, representing areas of the MEO particles that did not coalesce into a single solid solution during synthesis. The mixing entropy appear to not be high enough to form a single solid solution under typical synthesis conditions used during particle synthesis and requires increased temperatures during the heat treatment process. The lower entropy causes some elements to mix unevenly, resulting in added distortions to the crystal structure. The distortions can lead to additional peaks forming in the XRD pattern [29,31]. The STEM-EDS map displayed in Fig. 1D demonstrated that Ti, Mg, and O were well-mixed, with areas of Al not uniformly mixed showing that Al did not fully coalesce into the spinel phase. The uneven mixing seen in the STEM-EDS map confirms the additional peaks found in the XRD spectrum.

The XRD pattern of SPE-0, SPE-MEO-10, and SPE-MEO-60 are shown in Fig. 2D. SPE-0 has two main peaks located at 2θ of 19.09° and 23.26° which appear in all SPE samples. These two peaks are the result of the PEO crystalline phases in the polymer [32]. There was no discernible difference in XRD pattern between the SPE-0 and SPE-MEO-10 SPE. SPE-MEO-60 had several of the higher intensity peaks found in the MEO additive start to appear in the XRD pattern of the SPE. The appearance of MEO particle peaks in the XRD pattern of SPE-MEO-60 indicates the successful incorporation of the MEO additive into the polymer matrix. The presence of these peaks suggests that the MEO particles retained their crystal structure in the polymer and did not undergo significant chemical changes during the casting process.

3.2. Microscopy of PEO solid polymer electrolyte

The optical images for the SPE-0, SPE-MEO-10, and SPE-MEO-60 are shown in Fig. S4. The SPE are flexible and ranged in thickness from 153 to 247 μm. The morphology of the microsctructure for SPE-0, SPE-MEO-10, and SPE-MEO-60 are shown in Fig. 2A, B, and C, respectively. SPE-0 exhibits a spherulitic structure due to the addition of the LiTFSI salt [33]. As MEO is added to the PEO, the spherulitic structure reduces in size for SPE-MEO-10 and completely disappear in SPE-MEO-60 specimens. These spherulites can be corrolated to the crystalline phase in the PEO, and the decrease in their size suggest an increase in amorphous portion of PEO [34]. The high-resolution SEM image of the SPE is depicted in Fig. S5, which illustrates the disintegration of the spherulite structure with the addition of increasing amounts of MEO fillers.

3.3. Ionic conductivity of solid polymer electrolyte

Electrochemical impedance spectroscopy (EIS) was performed on all of the SPE to determine the bulk resistance of the membrane. EIS patterns for multiple test cells can be seen in Fig. S6 (SPE-0), Fig. S7 (SPE-Al_2O_3–10), Fig. S9 (SPE-MEO-10), and Fig. S10 (SPE-MEO-60) at temperatures ranging from 30 °C to 80 °C. The bulk resistance of each electrolyte decreases as the temperature increases and reaches a near-constant value around 50 °C, close to the melting temperature (T_m) of

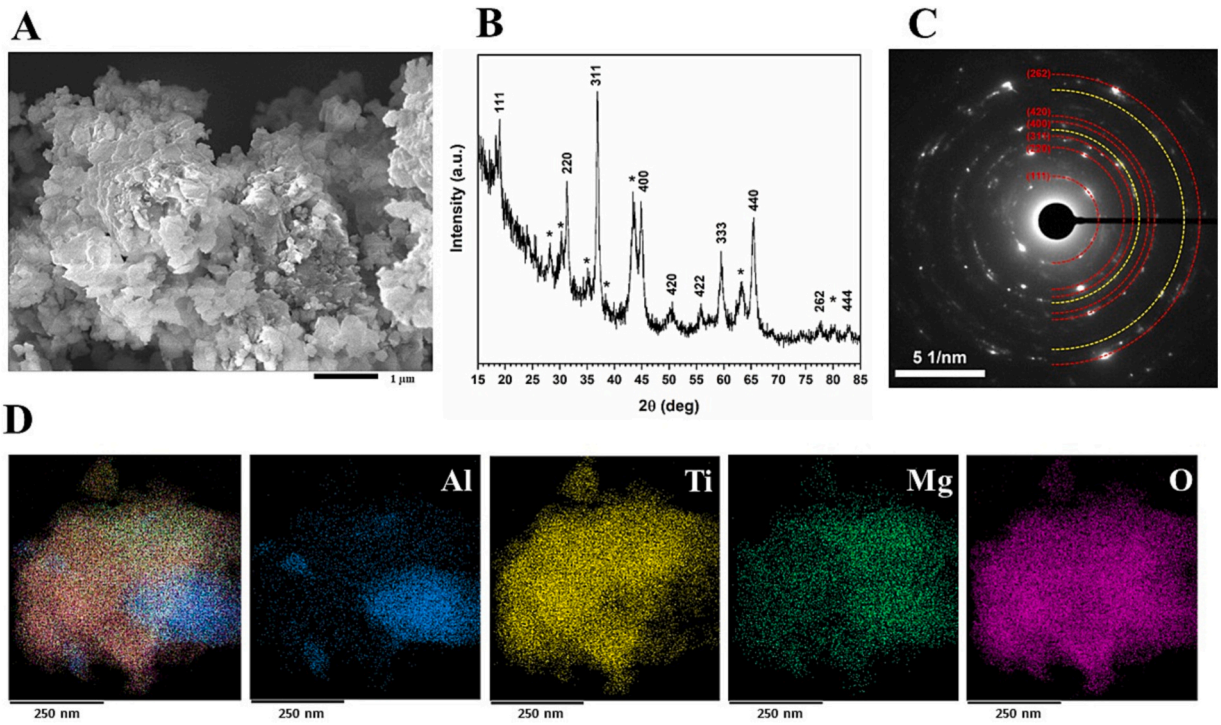

Fig. 1. Characterization of MEO powder (A) SEM. (B) XRD of AlTiMgLiO powder with assigned spinel phase planes. (C) SAED of AlTiMgLiO powder with selected planes. (D) Elemental mapping of AlTiMgLiO.

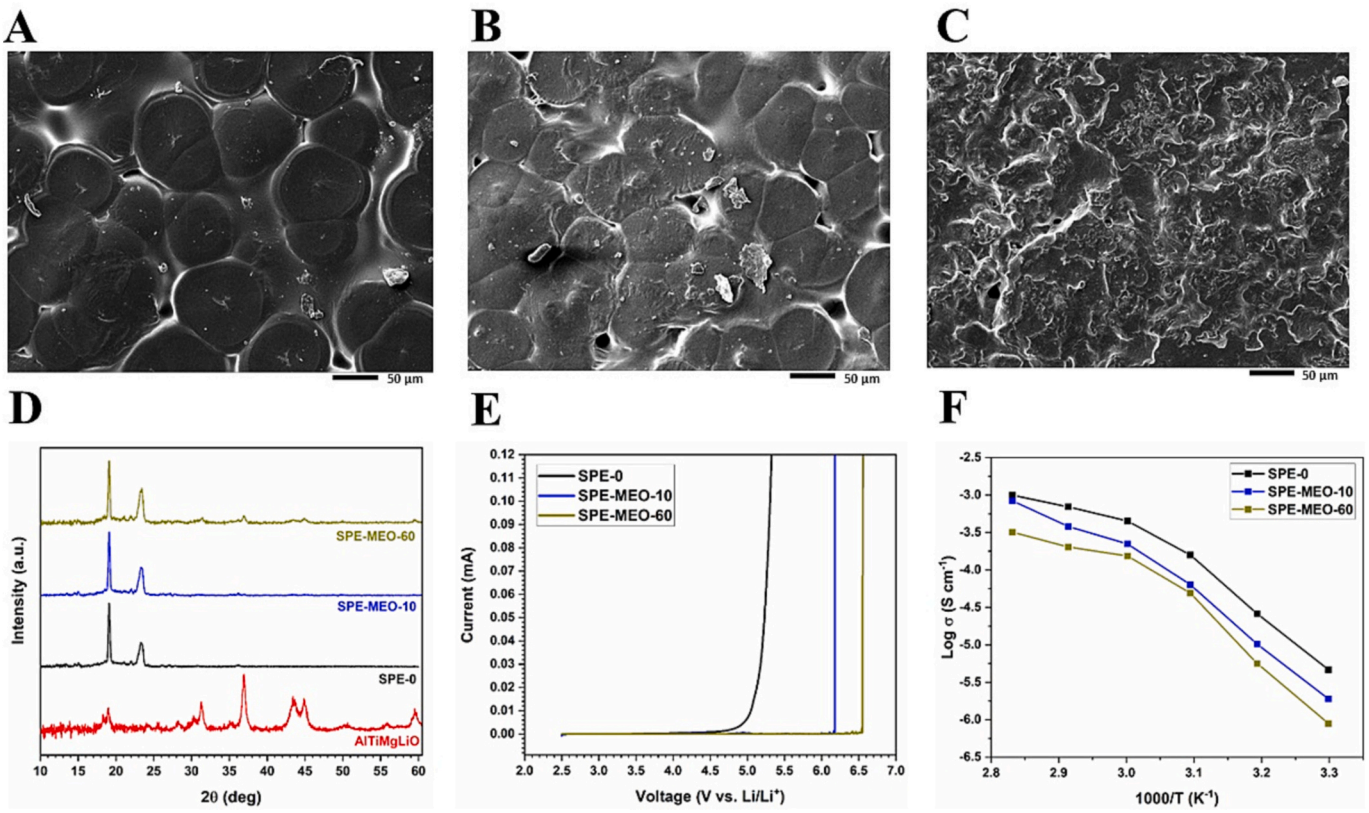

Fig. 2. Characterization of solid polymer electrolytes (A) SEM of SPE-0. (B) SEM of SPE-MEO-10. (C) SEM of SPE-MEO-60. (D) XRD of MEO, SPE-0, SPE-MEO-10, and SPE-MEO-60. (E) LSV of SPEs scanning from 2.5 to 7 V. (F) Arrhenius plot of SPEs ranging from 30 to 80 °C.

the PEO. Above T_m, the PEO becomes more amorphous, and its crystallinity increases below T_m, leading to changes in bulk resistance. The bulk resistance (R_b) and Eq. (1) were used to calculate the ionic conductivities at various temperatures, where L (cm) represents the thickness of the SPE, S (cm^2) represents the area of the stainless-steel electrode, and R_b (Ω) represents the bulk resistance of the electrolyte membrane, as measured by EIS.

$$\sigma = \frac{L}{R_b S} \tag{1}$$

Fig. 2F shows the plot of the ionic conductivities for SPE with varying MEO fillers. The ionic conductivity of SPE-0 is 4.65×10^{-6} S cm^{-1} at 30 °C and reaches a maximum of 9.94×10^{-4} S cm^{-1} at 80 °C. SPE-MEO-10 has an ionic conductivity of 2.00×10^{-6} S cm^{-1} at 30 °C and a maximum of 8.39×10^{-4} S cm^{-1} at 80 °C, while SPE-MEO-60 has an ionic conductivity of 7.73×10^{-7} S cm^{-1} at 30 °C and a maximum of 3.55×10^{-4} S cm^{-1} at 80 °C. Shown in Fig. S8, the ionic conductivity of SPE-Al_2O_3–10 is 1.39×10^{-6} S cm^{-1} at 30 °C and reaches a maximum of 6.78×10^{-4} S cm^{-1} at 80 °C. The ionic conductivity in SPE-MEO-10 is lower than that found in SPE-0 across all temperatures, and as more filler is added, the ionic conductivity is further reduced. Several factors contribute to the overall ionic conductivity found in a polymer. One factor could be related to the increase of mechanical properties of the electrolyte by the addition of fillers. A common explanation for ionic conductivity in PEO is attributed to the segmental motion of the amorphous regions [36,37]. It is well known that the increase in mechanical properties of polymer electrolytes can cause a decrease in ionic conductivity [35]. A stiffer electrolyte restricts the segmental motion in PEO and decreases the overall conductivity [38]. Similar results have shown that adding non-conducting fillers reduces conductivity in polymer electrolytes [39]. In this work, the designed SPE became stiffer as a result of more MEO being added, which can be a factor in the overall decrease in conductivity found in SPE-MEO-10 and SPE-MEO-60 electrolytes in comparison to the SPEs with no MEO fillers.

As shown in Fig. 2F, the ionic conductivities exhibit different slopes in the low-temperature regions (30 °C - 50 °C) compared to those in the high-temperature regions (60 °C - 80 °C). To analyze this difference, we calculated the activation energies for the SPE using Eq. (2), where A is the pre-exponential factor, k is the Boltzmann constant, σ is the ionic conductivity, and E_a is the activation energy for lithium-ion conduction [40].

$$\sigma = A\, exp\left(\frac{-E_a}{kT}\right) \tag{2}$$

The activation energies are summarized in Table 1, showing values ranging from 61.32 to 70.67 kJ mol^{-1} in the low-temperature region and 15.63–22.04 kJ mol^{-1} in the high-temperature region. The difference in activation energies is attributed to the recrystallization of PEO from the amorphous state when it is cooled to the transition temperature of 60 °C [8]. This crystallization leads to slower lithium transport through the PEO explained by the higher activation energy values at 30–50 °C [8]. In the 30-50℃ region, the addition of 10 wt.% MEO did not change the activation energy indicating that the ionic conductivity is still goverened by PEO.[34] However, the activation energy increased for SPE-MEO-60 specimens pointing to possible heterogeneous distribution of fillers in PEO that may cause agglomoration of fillers. At high temperatures, all SPE specimens showed decrease in activation energy, which is expected

Table 1
Activation Energy (E_a) summary for polymer electrolytes.

Electrolyte	Below melting point 30–50 °C /kJ mol^{-1}	Above melting point 60–80 °C / kJ mol^{-1}
SPE-0	62.38	16.82
SPE-MEO-10	61.32	22.04
SPE-MEO-60	70.67	15.63

in PEO materials due to ease of segmental motions.

3.4. Electrochemical performance of solid polymer electrolyte

3.4.1. Lithium transference number

The results of the DC polarization and impedance spectra are shown in Fig. S11. The calculated values for the lithium-ion transference number (t_{Li}^{+}) for SPE-0, SPE-MEO-10, and SPE-MEO-60 are summarized in Table 2. These values were calculated using Eq. (3), where currents I_o and I_{ss} represent the initial and steady state currents during DC polarization, and R_o and R_{ss} represent the electrode resistances before and after polarization, respectively [41].

$$t_{Li}^{+} = \frac{I_{ss}(\Delta V - I_o R_o)}{I_o(\Delta V - I_{ss} R_{ss})} \tag{3}$$

As seen in Table 2, the values for t_{Li}^{+} initially increase as more MEO is added, resulting in an increase in t_{Li}^{+} for SPE-MEO-10. This increase in transference number can be corrolated to higher dissociation of Li ions from their anion compartments in LiTFSI salts due to the presence of multielement particles. It is expected that the presence of Al, Ti and Mg cations in MEO results in stronger interactions with salt anions leading to more mobile Li ions. However, once the SPE reaches 60 wt%, the t_{Li}^{+} decreases to below the t_{Li}^{+} found in SPE-0. This decrease in t_{Li}^{+} is attributed to the filler having a blocking effect, resulting in higher scattering of Li ions moving across the SPE. The transference number has a large impact on the electrochemical performances of Li ion batteries [1]. According to simulations, a t_{Li}^{+} that approaches unity results in Li dendrite growth that theoretically stops as Li metal can be reversibly plated and stripped in the electrolyte [42]. The improvement to t_{Li}^{+} in SPE-MEO-10 should slow down Li dendrite growth compared to SPE-0.

3.4.2. Linear sweep voltammetry

The electrochemical stability of the SPE is an important parameter to determine practical applications as an electrolyte in lithium-ion batteries. To determine the stability of the SPE, linear sweep voltammetry (LSV) was performed. As shown in Fig. 2E, both SPE-MEO-10 and SPE-MEO-60 are found to be more stable than SPE-0. There was no anodic current in SPE-MEO-10 until 6.18 V, and SPE-MEO-60 showed no current until 6.55 V. SPE-0 started showing current flow at 4.66 V. Above these voltages, the SPE will start to decompose due to oxidation reactions. The larger voltage window is attributed to the MEO additive of Al, Ti, and Mg, as such metal oxides are known to be good insulators due to high resistivity and high dielectric constants [43–46]. The higher stability voltage windows found in the SPE-MEO-10 and SPE-MEO-60 indicate the potential of MEO-polymer composites for use in high voltage lithium batteries.

3.4.3. Voltage polarization

To further study the electrochemical stability of the SPE, the voltage polarization of the SPE was investigated. Fig. 3 shows the overpotential values with a current density of 20 μA cm^{-2}. SPE-0 had an average over potential of −10.66 mV on the negative potential and 10.10 mV on the positive potential, with an absolute min of −12.1 mV and an absolute max of 11.6 mV. SPE-Al_2O_3–10 had an average over potential of −12.40 mV on the negative potential and 11.36 mV on the positive potential, with an absolute min of −17.5 mV and an absolute max of 15.1 mV. SPE-MEO-10 showed a lower average over potential of −8.80 mV on the negative potential and 7.97 mV on the positive potential with an absolute min of −9.35 mV and an absolute max of 8.45 mV. The lower overpotential values in SPE-MEO-10 indicates a higher ease of deposition/stripping from the foil surface for the SPE with the MEO fillers [28]. The increasing overpotential increasing with cycle number found in SPE-0 during the first 33 h and in SPE-Al_2O_3–10 during the first 14 h is an indication of a thick and growing interfacial layers due to uneven lithium plating that can be detrimental for further cycling [28]. SPE-Al_2O_3–10 shows a sharp increase in the overpotential in the initial cycles and a higher overpotential overall, highlighting fast growing interfacial layers likely due to dendrite formation. SPE-MEO-10 shows a slower increasing overpotential with increasing cycle number indicating more uniform growth of the interfacial layer indicative of less Li dendritic behavior. The voltage polarization remained stable through 500 cycles and shows safe operation along with the ability to block lithium dendrite penetration over long cycles [47] Section 3.5.

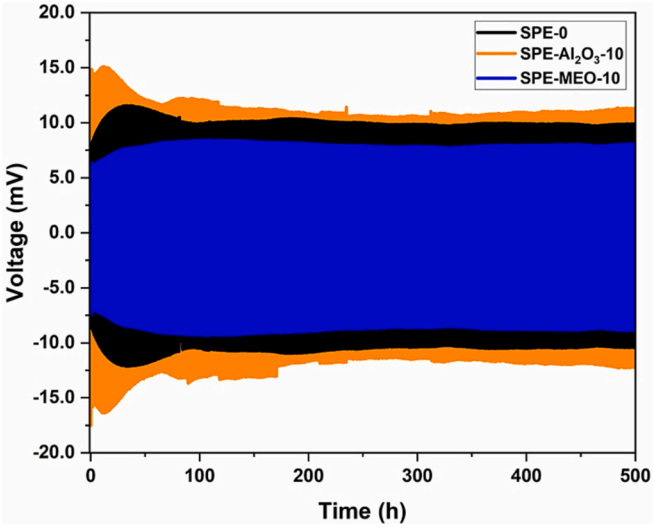

Fig. 3. Voltage polarization versus time for SPE-0 (black), SPE-Al_2O_3-10 (orange), and SPE-MEO-10 (blue) solid polymer electrolytes at 20 μA cm^{-2}. (For interpretation of the references to colour in this figure legend, the reader is referred to the web version of this article.)

3.4.4. Cycling performance of solid polymer electrolyte

The electrochemical properties of SPE composites were further studied by investigating the cycling characteristics during charge/discharge. Fig. 4 shows the charge-discharge profile and cycling performance of SPE-0, SPE-Al_2O_3-10 and SPE-MEO-10. The cycling performance of SPE-MEO-60 was not included due to initial characterization of the electrolyte which resulted in higher resistance values and lower ionic conductivity, lower transference number, and poorer morphology. The voltage profiles for selected cycles are shown in Fig. 4A, B and C. During the first 50 cycles, SPE-MEO-10 had a much smaller capacity loss than both SPE-0 and SPE-Al_2O_3–10. SPE-Al_2O_3–10 showed a slight improvement in capacity loss over SPE-0. In cycle 1, SPE-0 had an initial capacity of 140.30 mAh g^{-1}, which reduced to 123.12 mAh g^{-1} in cycle 50, resulting in a reduction of 17.17 mAh g^{-1} (−12.24 %). The unary SPE-Al_2O_3–10 had an initial capacity of 144.25 mAh g^{-1} in cycle 1 and reduced to 128.94 mAh g^{-1} after 50 cycles, a reduction of 15.32 mAh g^{-1} (−10.61 %). The unary additive was a slight improvement over SPE-0 during the first 50 cycles. However, SPE-MEO-10 had an initial capacity of 126.67 mAh g^{-1} in cycle 1 and reduced to 121.76 mAh g^{-1} after 50 cycles, a reduction of only 4.91 mAh g^{-1} (−3.88 %). Fig. 5 highlights the capacity loss by cycling region and shows not only a lower decrease across all regions in SPE-MEO-10 but a substantial improvement in the first 50 cycles compared to SPE-0 and

Table 2
Measured values of parameters from Eq. 3 with corresponding lithium ion transference numbers (t_{Li}^{+}) at 80 °C.

Electrolyte	I_o / mA	I_{ss} / mA	R_o / Ω	R_{ss} / Ω	ΔV / mV	t_{Li}^{+}
SPE-0	0.0858	0.0530	65.50	51.33	10	0.37
SPE-MEO-10	0.0870	0.0475	48.70	51.16	10	0.42
SPE-MEO-60	0.0818	0.0401	65.97	70.99	10	0.31

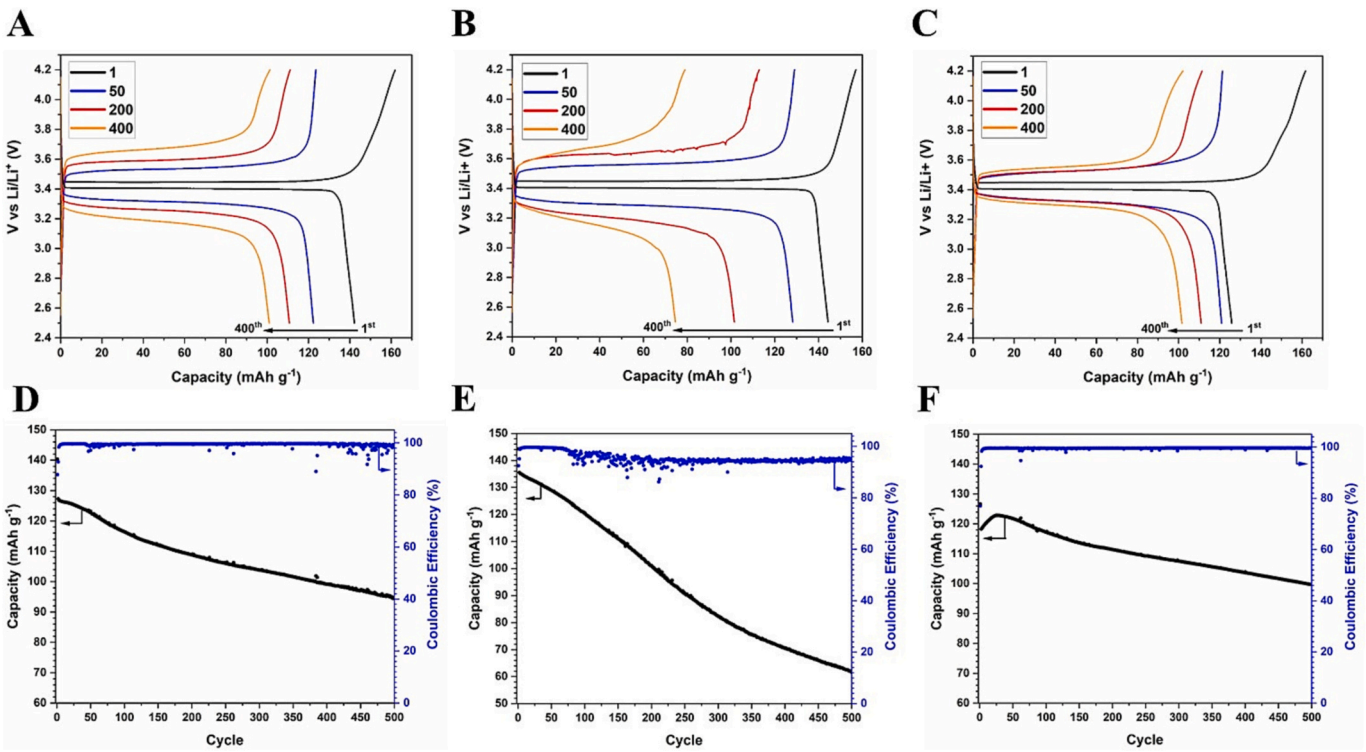

Fig. 4. Electrochemical performance for $LiFePO_4$|SPE|Li at 80 °C and 1C. Galvanostatic charge/discharge of select cycles for (A) SPE-0. (B) SPE-Al_2O_3-10. (C) SPE-MEO-10. Cycling performance and Coulombic efficiency of (D) SPE-0 (E) SPE-Al_2O_3-10 (F) SPE-MEO-10.

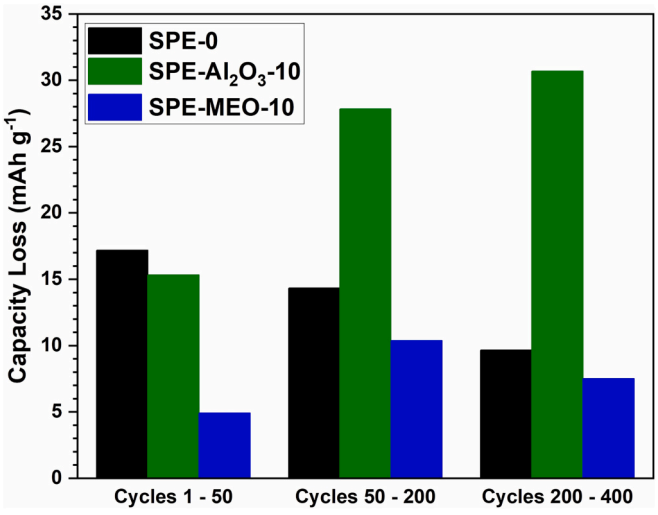

Fig. 5. Discharge capacity loss per cycling region.

SPE-Al_2O_3–10. The long-term cycling for SPE-0, SPE-Al_2O_3–10 and SPE-MEO-10 are shown in Fig. 4D, E, and F. SPE-MEO-10 had a lower initial capacity than SPE-0 and SPE-Al_2O_3–10 (126.67 vs 140.30 mAh g^{-1} and 144.25 mAh g^{-1}) due to the decrease in conductivity of the SPE, but it exhibited better long-term cycling performance than the other two SPE. At higher charging rates, the lower conductivity causes the cell to run into transport issues as ions cannot move fast enough through the electrolyte. The higher resistance values in the electrolyte, coupled with higher charging rates, result in higher ohmic losses, which cause higher voltage drops. The lower cutoff voltage is reached faster, resulting in a lower overall capacity. Similar phenomenon have been reported in other systems where there is a loss in capacity due to lower ionic conductivity at higher charging rates [48]. However, the MEO additive in SPE-MEO-10 had a positive effect on the overall stability of the cells, causing less capacity loss per cycle than SPE-0 and SPE-Al_2O_3–10. SPE-0 had a maximum capacity of 140.30 mAh g^{-1} and a capacity of 94.66 mAh g^{-1} after 500 cycles, resulting in a capacity retention of 64.47 %. The unary electrolyte, SPE-Al_2O_3–10, had a maximum capacity of 144.25 mAh g^{-1} and a capacity of 61.53 mAh g^{-1} after 500 cycles, resulting in a capacity retention of 42.65 %. SPE-Al_2O_3–10 had a lower average Coulombic efficiency and more variability than both SPE-0 and SPE-MEO-10. In contrast, SPE-MEO-10 had a maximum capacity of 126.67 mAh g^{-1} and a capacity of 99.68 mAh g^{-1} after 500 cycles, resulting in a capacity retention of 78.69 %. The MEO additive in SPE-MEO-10 resulted in a 14.2 % increase in capacity retention and 5.03 mAh g^{-1} increase in overall capacity over 500 cycles, demonstrating stable interfacial layers and better lithium plating due to the MEO fillers. In addition, the Coulombic efficiency was not only higher in SPE-MEO-10 but was more stable over the 500 cycles compared to SPE-0 and SPE-Al_2O_3–10.

3.5. Morphology changes in cycled cells

The differences in capacity degradation were studied further by observing the Li anode after cycling. SPE-0, SPE-MEO-10 and SPE-Al_2O_3-10 were cycled for 100 cycles to compare how the surface morphology changes during cycling. Fig. 6 shows a comparison of the Li anode for different electrolytes. Fig. 6A and E shows the surface morphology of a fresh Li anode that was not cycled. Here, you can observe a fairly rough and uneven surface before any cycling has occurred. Fig. 6B and F shows the Li anode of a cell cycled with SPE-0. The Li anode shares a similar rough and uneven surface as the fresh Li surface but is thicker and more interconnected, representing uneven growth of the lithium morphology. Fig. 6C and G shows the Li anode of a cell cycled with SPE-Al_2O_3–10. The surface is covered by a thick layer of growth. The morphology found in the fresh Li anode are no longer observable in SPE-Al_2O_3–10 and have become covered by the formed interfacial layer. The SPE-Al_2O_3–10 shows some evidence of uneven lithium plating explaining the resulting poor capacity retention.

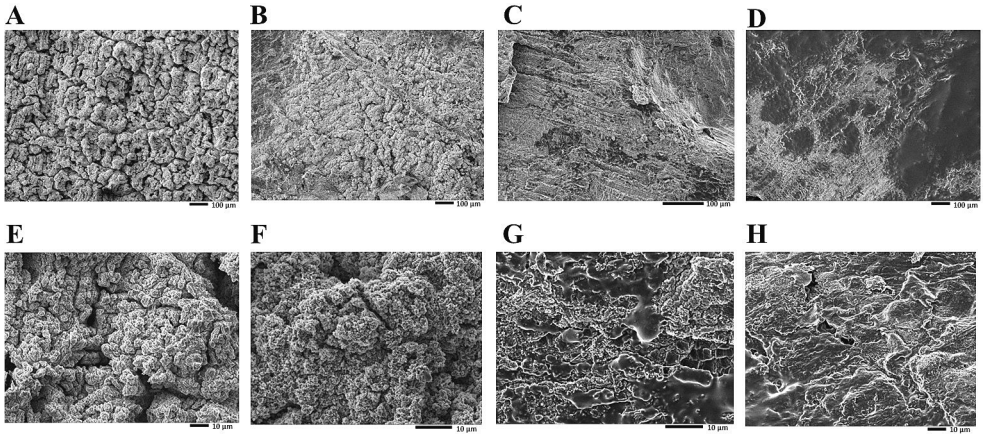

Fig. 6. SEM morphology of Li anodes after 100 cycles with low and high magnification. (A & E) Uncycled Li anode. (B & F) SPE-0. (C & G) SPE-Al_2O_3-10. (D & H) SPE-MEO-10.

Fig. 6D and H shows the Li anode of a cell cycled with SPE-MEO-10. Here, a dense uniform lithium morphology is observed pointing to the ability of SPE-MEO-10 electrolytes to suppress the dendritic lithium. In a study with silica, these particles improved cycle life and was attributed to the formation of a smoother and denser layer as observed by SEM [49]. The MEO filler allows for a slower, more uniform interfacial layer to form and grow, reducing capacity degradation over time.

3.6. *Mechanisms for reduced dendritic growth*

The increase in cycling stability is attributed to the enhanced suppression of lithium dendrites achieved through increased mechanical stiffness of SPE-MEO-10 and also the presence of multielement particles in the electrolyte. Recent research on lithium dendrite growth indicates that even minor stresses and imperfections on a surface can initiate and propagate Li dendrite formation [50]. Thus, relying solely on the strategy of eliminating imperfections may not be practical for large-scale manufacturing of LIBs. High molecular weight polymers like PEO demonstrate thermodynamic stability with Li up to temperatures as high as 100 °C [51]. With minimal interfacial reaction between PEO and fresh Li, the primary factor limiting the cycle life of Li metal anodes is Li dendrite growth [1]. It has been demonstrated that PEO alone cannot effectively block dendrite growth, particularly at elevated temperatures when the strength of PEO significantly diminishes [1,52]. However, mechanical blocking is a viable method that can reduce lithium dendrite growth and improve cycle life [1]. Additionally, multielement materials exhibit synergistic effects, enhancing the polymer's electrochemical properties. The mechanism for improvement in lithium plating with multielement particles can be seen in Fig. 7. In Fig. 7A, an uncycled Li anode with a SPE is shown. The Li anode surface has an relatively flat morphology before any cycling occurs. Fig. 7B. shows the case for SPE-0 when no MEO particles are used. The SPE is not mechanically strong enough to suppress the formation of the interfacial layer and also does not have high selectivity for mobile lithium or voltage stability as we see in composite electrolyte cases, resulting in dendritic lithium morphology. Fig. 7C shows the case for SPE-Al_2O_3–10 composites when Al_2O_3 fillers were used. The Al_2O_3 fillers are mechanically strong enough to suppress the dendritic growth, which causes different areas of the Li anode to grow at different rates until a uniform layer is formed. While Al_2O_3 particles are able to increase the mechanical properties of the SPE, the electrochemical properties of the SPE are negatively affected, making it incompetent to fully reduce uneven lithium deposition, resulting in the cycling capacity being greatly reduced. Fig. 7D shows the case for SPE-MEO-10 when MEO particles are used. The increase of mechanical properties in SPE-MEO-10, along with the improvement in mobile lithium selectivity (transference number) and better stability under the electrochemical chanrge/discharge window, allows for more uniform lithium plating and stripping behavior. The improvements to the lithium morphology result in improved capacity retention and longer life during cycling for SPE-MEO-10.

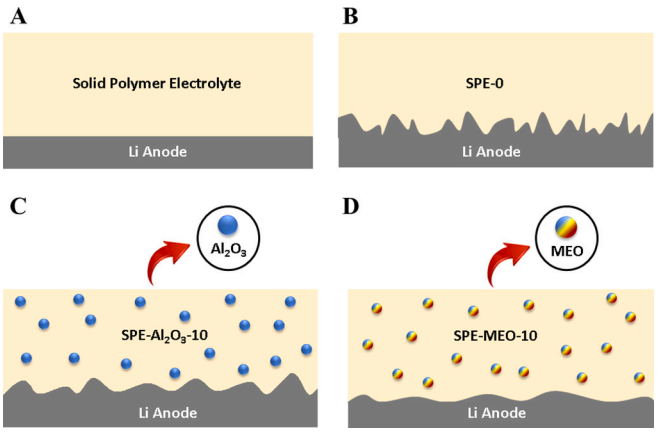

Fig. 7. Mechanism for reduction in dendritic growth with (A) fresh Li anode. (B) Cycled Li anode with SPE-0. (C) Cycled Li anode with SPE-Al_2O_3-10. (D) Cycled Li anode SPE-MEO-10.

4. Conclusions

Solid polymer electrolytes composed of PEO and multielement oxide fillers consisting of AlTiMgLiO were synthesized and characterized. XRD and EDS confirmed the presence and distribution of the elements, revealing that a single solid solution did not form, unlike in the case of high entropy materials. This lack of formation can be attributed to the absence of additional elements or the need for higher temperatures during the synthesis process. The optimized concentration, identified as SPE-MEO-10, improved the electrochemical properties. This led to an enhanced lithium transference number of 0.42 and an increase of the electrochemical stability of SPE-MEO-10 from 4.66 V to 6.18 V vs Li^+/Li. With the addition of MEO fillers, a smoother and more uniform lithium deposition forms explaining the improved electrochemical performance. The improved lithium plating and stripping contributed to enhanced cycling characteristics, with SPE-MEO-10 having a capacity of 99.68 mAh g^{-1} after 500 cycles and a capacity retention of 78.69 %. Furthermore, the Coulombic efficiency also showed improvement reaching an average of 99.46 % over 500 cycles. Our work demonstrates that fillers based on multielement materials have the potential to

enhance the cycling and capacity retention of polymer electrolytes in lithium batteries.

CRediT authorship contribution statement

T.G.R. developed the concept, designed the experiment, analyzed the experimental data, and performed the XRD characterization. J.M.G contributed to developing the polymer synthesis process. S.S. analyzed part of the cycling data and provided components for testing. A.G. performed the electron microscopy and EDS spectroscopy. T.S. provided instrument support. R.S.Y. directed the project. T.G.R and R.S.Y wrote the paper. All authors discussed the results and commented on the manuscript.

Declaration of competing interest

The authors declare no conflict of interest.

Data availability

Data will be made available on request.

Acknowledgments

The authors acknowledge partial financial support from National Science Foundation CBET-2313395. In addition, we thank the fellowship granted to J.M.G. (FAPESP 2020/06176-7 and 2018/16896-7). This work made use of instruments in the Electron Microscopy Core of UIC's Research Resources Center. This work made use of XRD at the Nanotechnology Core Facility at UIC.

Appendix A. Supplementary data

Supplementary data to this article can be found online at https://doi.org/10.1016/j.est.2023.108491.

References

[1] W. Xu, J. Wang, F. Ding, X. Chen, E. Nasybulin, Y. Zhang, et al., Lithium metal anodes for rechargeable batteries, Energy Environ. Sci. 7 (2014) 513–537, https://doi.org/10.1039/c3ee40795k.
[2] X. Chen, W. He, L.X. Ding, S. Wang, H. Wang, Enhancing interfacial contact in all solid state batteries with a cathode-supported solid electrolyte membrane framework, Energy Environ. Sci. 12 (2019) 938–944, https://doi.org/10.1039/c8ee02617c.
[3] S. Choudhury, S. Stalin, D. Vu, A. Warren, Y. Deng, P. Biswal, et al., Solid-state polymer electrolytes for high-performance lithium metal batteries, Nat. Commun. 10 (2019) 1–8, https://doi.org/10.1038/s41467-019-12423-y.
[4] D. Dong, B. Zhou, Y. Sun, H. Zhang, G. Zhong, Q. Dong, et al., Polymer electrolyte glue: a universal interfacial modification strategy for all-solid-state Li batteries, Nano Lett. 19 (2019) 2343–2349, https://doi.org/10.1021/acs.nanolett.8b05019.
[5] J.Y. Song, Y.Y. Wang, C.C. Wan, Review of gel-type polymer electrolytes for lithium-ion batteries, J. Power Sources 77 (1999) 183–197, https://doi.org/10.1016/S0378-7753(98)00193-1.
[6] J. Mindemark, M.J. Lacey, T. Bowden, D. Brandell, Beyond PEO—alternative host materials for Li+-conducting solid polymer electrolytes, Prog. Polym. Sci. 81 (2018) 114–143, https://doi.org/10.1016/j.progpolymsci.2017.12.004.
[7] P. Yao, H. Yu, Z. Ding, Y. Liu, J. Lu, M. Lavorgna, et al., Review on polymer-based composite electrolytes for Lithium batteries, Front. Chem. 7 (2019) 1–17, https://doi.org/10.3389/fchem.2019.00522.
[8] J.H. Choi, C.H. Lee, J.H. Yu, C.H. Doh, S.M. Lee, Enhancement of ionic conductivity of composite membranes for all-solid-state lithium rechargeable batteries incorporating tetragonal Li7La3Zr2O12 into a polyethylene oxide matrix, J. Power Sources 274 (2015) 458–463, https://doi.org/10.1016/j.jpowsour.2014.10.078.
[9] Q. Zhou, J. Ma, S. Dong, X. Li, G. Cui, Intermolecular chemistry in solid polymer electrolytes for high-energy-density lithium batteries, Adv. Mater. 31 (2019) 1–21, https://doi.org/10.1002/adma.201902029.
[10] M. Ebadi, C. Marchiori, J. Mindemark, D. Brandell, C.M. Araujo, Assessing structure and stability of polymer/lithium-metal interfaces from first-principles calculations, J. Mater. Chem. A 7 (2019) 8394–8404, https://doi.org/10.1039/c8ta12147h.
[11] C. Wang, T. Wang, L. Wang, Z. Hu, Z. Cui, J. Li, et al., Differentiated lithium salt design for multilayered PEO electrolyte enables a high-voltage solid-state lithium metal battery, Adv. Sci. 6 (2019), https://doi.org/10.1002/advs.201901036.
[12] J. Wu, Z. Rao, Z. Cheng, L. Yuan, Z. Li, Y. Huang, Ultrathin, flexible polymer electrolyte for cost-effective fabrication of all-solid-state lithium metal batteries, Adv. Energy Mater. 9 (2019) 1–8, https://doi.org/10.1002/aenm.201902767.
[13] X. Zhang, S. Wang, C. Xue, C. Xin, Y. Lin, Y. Shen, et al., Self-suppression of lithium dendrite in all-solid-state lithium metal batteries with poly(vinylidene difluoride)-based solid electrolytes, Adv. Mater. 31 (2019) 1–9, https://doi.org/10.1002/adma.201806082.
[14] A.Y. Jee, H. Lee, Y. Lee, M. Lee, Determination of the elastic modulus of poly (ethylene oxide) using a photoisomerizing dye, Chem. Phys. 422 (2013) 246–250, https://doi.org/10.1016/j.chemphys.2012.12.028.
[15] X. Pan, P. Yang, Y. Guo, K. Zhao, B. Xi, F. Lin, et al., Electrochemical and nanomechanical properties of TiO2 ceramic filler Li-ion composite gel polymer electrolytes for Li metal batteries, Adv. Mater. Interfaces 8 (2021) 48–50, https://doi.org/10.1002/admi.202100669.
[16] J. Feng, L. Wang, Y. Chen, P. Wang, H. Zhang, X. He, PEO based polymer-ceramic hybrid solid electrolytes: a review, Nano Converg. 8 (2021), https://doi.org/10.1186/s40580-020-00252-5.
[17] W. Liu, S.W. Lee, D. Lin, F. Shi, S. Wang, A.D. Sendek, et al., Enhancing ionic conductivity in composite polymer electrolytes with well-aligned ceramic nanowires, Nat. Energy 2 (2017) 1–7, https://doi.org/10.1038/nenergy.2017.35.
[18] J.M.C. Puguan, W.J. Chung, H. Kim, Ion-conductive and transparent PVdF-HFP/silane-functionalized ZrO2 nanocomposite electrolyte for electrochromic applications, Electrochim. Acta 196 (2016) 236–244, https://doi.org/10.1016/j.electacta.2016.02.172.
[19] A. Manuel Stephan, K.S. Nahm, Review on composite polymer electrolytes for lithium batteries, Polymer (Guildf) 47 (2006) 5952–5964, https://doi.org/10.1016/j.polymer.2006.05.069.
[20] N.T. Kalyana Sundaram, A. Subramania, Nano-size LiAlO2 ceramic filler incorporated porous PVDF-co-HFP electrolyte for lithium-ion battery applications, Electrochim. Acta 52 (2007) 4987–4993, https://doi.org/10.1016/j.electacta.2007.01.066.
[21] A.M. Christie, S.J. Lilley, E. Staunton, Y.G. Andreev, P.G. Bruce, Increasing the conductivity of crystalline polymer electrolytes, Nature. 433 (2005) 50–53, https://doi.org/10.1038/nature03186.
[22] M. Moreno, R. Quijada, M.A. Santa Ana, E. Benavente, P. Gomez-Romero, G. González, Electrical and mechanical properties of poly(ethylene oxide)/intercalated clay polymer electrolyte, Electrochim. Acta 58 (2011) 112–118, https://doi.org/10.1016/j.electacta.2011.08.096.
[23] X.W. Zhang, C. Wang, A.J. Appleby, F.E. Little, Characteristics of lithium-ion-conducting composite polymer-glass secondary cell electrolytes, J. Power Sources 112 (2002) 209–215, https://doi.org/10.1016/S0378-7753(02)00365-8.
[24] A.H. Phakatkar, T. Shokuhfar, R. Shahbazian-Yassar, Nanoscale chemical and structural investigation of solid solution polyelemental transition metal oxide nanoparticles, iScience 26 (2023), 106032, https://doi.org/10.1016/j.isci.2023.106032.
[25] A. Sarkar, Q. Wang, A. Schiele, M.R. Chellali, S.S. Bhattacharya, D. Wang, et al., High-entropy oxides: fundamental aspects and electrochemical properties, Adv. Mater. 31 (2019), https://doi.org/10.1002/adma.201806236.
[26] D. Bérardan, S. Franger, D. Dragoe, A.K. Meena, N. Dragoe, Colossal dielectric constant in high entropy oxides, Phys. Status Solidi Rapid Res. Lett. 10 (2016) 328–333, https://doi.org/10.1002/pssr.201600043.
[27] J. Dąbrowa, M. Stygar, A. Mikuła, A. Knapik, K. Mroczka, W. Tejchman, et al., Synthesis and microstructure of the (Co,Cr,Fe,Mn,Ni)3O4 high entropy oxide characterized by spinel structure, Mater. Lett. 216 (2018) 32–36, https://doi.org/10.1016/j.matlet.2017.12.148.
[28] R. Deivanayagam, R. Shahbazian-Yassar, Electrochemical methods and protocols for characterization of ceramic and polymer electrolytes for rechargeable batteries, Batter Supercaps. 4 (2021) 596–606, https://doi.org/10.1002/batt.202000221.
[29] A.H. Phakatkar, M.T. Saray, G. Rasul, L.V. Sorokina, T. Ritter, T. Shokuhfar, et al., Ultrafast synthesis of high entropy oxide nanoparticles by flame spray pyrolysis, Langmuir. (2021), https://doi.org/10.1021/acs.langmuir.1c01105.
[30] T.G. Ritter, A.H. Phakatkar, M.G. Rasul, M.T. Saray, L.V. Sorokina, T. Shokuhfar, et al., Electrochemical synthesis of high entropy hydroxides and oxides boosted by hydrogen evolution reaction, Cell Rep. Phys. Sci. 3 (2022), 100847, https://doi.org/10.1016/j.xcrp.2022.100847.
[31] L. Kalinowski, J. Goraus, A. Slebarski, "DistorX" program for analysis of structural distortions affecting X-ray diffraction patterns, AIP Adv. 8 (2018), https://doi.org/10.1063/1.5042654.
[32] K.M. Freitag, H. Kirchhain, L. van Wüllen, T. Nilges, Enhancement of Li ion conductivity by electrospun polymer fibers and direct fabrication of solvent-free separator membranes for Li ion batteries, Inorg. Chem. 56 (2017) 2100–2107, https://doi.org/10.1021/acs.inorgchem.6b02781.
[33] J. Gurusiddappa, W. Madhuri, R. Padma Suvarna, Dasan K. Priya, Studies on the morphology and conductivity of PEO/LiClO4, Mater. Today Proc. 3 (2016) 1451–1459, https://doi.org/10.1016/j.matpr.2016.04.028.
[34] T.M.W.J. Bandara, D.G.N. Karunathilaka, J.L. Ratnasekera, L. Ajith De Silva, A. C. Herath, B.E. Mellander, Electrical and complex dielectric behaviour of composite polymer electrolyte based on PEO, alumina and tetrapropylammonium iodide, Ionics (Kiel) 23 (2017) 1711–1719, https://doi.org/10.1007/s11581-017-2016-y.
[35] S. Berg, T. Kelly, I. Porat, B. Moradi-Ghadi, H. Ardebili, Mechanical deformation effects on ion conduction in stretchable polymer electrolytes, Appl. Phys. Lett. 113 (2018), https://doi.org/10.1063/1.5040368.
[36] B. Kumar, S.J. Rodrigues, S. Koka, The crystalline to amorphous transition in PEO-based composite electrolytes: role of lithium salts, Electrochim. Acta 47 (2002) 4125–4131, https://doi.org/10.1016/S0013-4686(02)00442-5.

[37] S.K. Fullerton-Shirey, J.K. Maranas, Effect of LiClO 4 on the structure and mobility of PEO-based solid polymer electrolytes, Macromolecules. 42 (2009) 2142–2156, https://doi.org/10.1021/ma802502u.
[38] Y.A. Samad, A. Asghar, B.S. Lalia, R. Hashaikeh, Networked cellulose entrapped and reinforced PEO-based solid polymer electrolyte for moderate temperature applications, J. Appl. Polym. Sci. 129 (2013) 2998–3006, https://doi.org/10.1002/app.39033.
[39] S. Kalnaus, A.S. Sabau, W.E. Tenhaeff, N.J. Dudney, C. Daniel, Design of composite polymer electrolytes for Li ion batteries based on mechanical stability criteria, J. Power Sources 201 (2012) 280–287, https://doi.org/10.1016/j.jpowsour.2011.11.020.
[40] Y. Zhao, C. Wu, G. Peng, X. Chen, X. Yao, Y. Bai, et al., A new solid polymer electrolyte incorporating Li10GeP2S12 into a polyethylene oxide matrix for all-solid-state lithium batteries, J. Power Sources 301 (2016) 47–53, https://doi.org/10.1016/j.jpowsour.2015.09.111.
[41] S. Zugmann, M. Fleischmann, M. Amereller, R.M. Gschwind, H.D. Wiemhöfer, H. J. Gores, Measurement of transference numbers for lithium ion electrolytes via four different methods, a comparative study, Electrochim. Acta 56 (2011) 3926–3933, https://doi.org/10.1016/j.electacta.2011.02.025.
[42] C. Monroe, J. Newman, Dendrite growth in lithium/polymer systems, J. Electrochem. Soc. 150 (2003) A1377, https://doi.org/10.1149/1.1606686.
[43] R.F. Cava, W.F. Peck, J.J. Krajewski, Enhancement of the dielectric constant of Ta2O5 through substitution with TiO2, Nature. 377 (1995) 215–217, https://doi.org/10.1038/377215a0.
[44] J. Hornak, P. Trnka, P. Kadlec, O. Michal, V. Mentlík, P. Šutta, et al., Magnesium oxide nanoparticles: dielectric properties, surface functionalization and improvement of epoxy-based composites insulating properties, Nanomaterials. 8 (2018) 1–17, https://doi.org/10.3390/nano8060381.
[45] J. Kolodzey, E.A. Chowdhury, T.N. Adam, G. Qui, I. Rau, J.O. Olowolafe, et al., Electrical conduction and dielectric breakdown in aluminum oxide insulators on silicon, IEEE Trans. Electron. Devices 47 (2000), 121128.
[46] Y. Ju, T. Chen, Z. Wu, Y. Jiang, Electrical properties of amorphous titanium oxide thin films, Bandaoti Guangdian/Semiconductor Optoelectron. 33 (2012) 676–679.
[47] R. Rojaee, S. Plunkett, M.G. Rasul, M. Cheng, V. Jabbari, R. Shahbazian-Yassar, Interfacial engineering of lithium-polymer batteries with in situ UV cross-linking, InfoMat. 3 (2021) 1016–1027, https://doi.org/10.1002/inf2.12197.
[48] Y. Orikasa, Y. Gogyo, H. Yamashige, M. Katayama, K. Chen, T. Mori, et al., Ionic conduction in lithium ion battery composite electrode governs cross-sectional reaction distribution, Sci. Rep. 6 (2016) 2–7, https://doi.org/10.1038/srep26382.
[49] X.-W. Zhang, Y. Li, S.A. Khan, P.S. Fedkiw, Inhibition of lithium dendrites by fumed silica-based composite electrolytes, J. Electrochem. Soc. 151 (2004) A1257, https://doi.org/10.1149/1.1767158.
[50] G. McConohy, X. Xu, T. Cui, E. Barks, S. Wang, E. Kaeli, et al., Mechanical regulation of lithium intrusion probability in garnet solid electrolytes, Nat. Energy (2023), https://doi.org/10.1038/s41560-022-01186-4.
[51] K. Zaghib, M. Armand, M. Gauthier, Electrochemistry of anodes in solid-state Li-ion polymer batteries, J. Electrochem. Soc. 145 (1998) 3135–3140, https://doi.org/10.1149/1.1838776.
[52] B. Scrosati, A. Selvaggi, F. Croce, W. Gang, The Li/LiV3O8 polymer electrolyte lithium battery III. Investigation of the electrode interfaces, J. Power Sources 24 (1988) 287–294, https://doi.org/10.1016/0378-7753(88)80104-6.